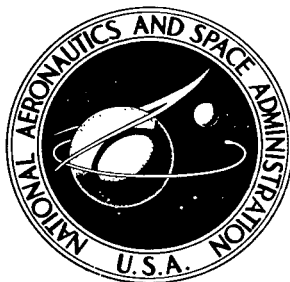


NASA TECHNICAL NOTE



NASA TN D-4743

*c.1*

NASA TN D-4743



STRESS-STRAIN BEHAVIOR OF COLD-WELDED  
COPPER-COPPER MICROJUNCTIONS IN VACUUM  
AS DETERMINED FROM ELECTRICAL  
RESISTANCE MEASUREMENTS

LOAN COPY: RETURN TO  
AFWL (WLIL-2)  
KIRTLAND AFB, N MEX

*by John S. Przybyszewski*

*Lewis Research Center  
Cleveland, Ohio*



STRESS-STRAIN BEHAVIOR OF COLD-WELDED COPPER-COPPER  
MICROJUNCTIONS IN VACUUM AS DETERMINED FROM  
ELECTRICAL RESISTANCE MEASUREMENTS

By John S. Przybyszewski

Lewis Research Center  
Cleveland, Ohio

NATIONAL AERONAUTICS AND SPACE ADMINISTRATION

---

For sale by the Clearinghouse for Federal Scientific and Technical Information  
Springfield, Virginia 22151 - CFSTI price \$3.00

## ABSTRACT

True stress-strain curves, developed from contact-resistance measurements between two OFHC copper specimens loaded and unloaded in vacuum, showed that the cold-welded junctions exhibited an amount of ductility generally characteristic of the specimen material. Junction ductility was greater when the experiment was kept vibration free. Deliberate vibration introduced during the loading cycle lowered the junction ductility. The contact-resistance-against-load data also seemed to indicate that impulsive forces could increase the area of contact under fixed load to a point where the contact area might revert to an elastic condition.

STRESS-STRAIN BEHAVIOR OF COLD-WELDED COPPER-COPPER  
MICROJUNCTIONS IN VACUUM AS DETERMINED FROM  
ELECTRICAL RESISTANCE MEASUREMENTS

by John S. Przybyszewski

Lewis Research Center

SUMMARY

Continuous x, y-recordings were made of the contact resistance against the load for two oxygen-free high-conductivity (OFHC) copper specimens (hemisphere against cylinder) compressively loaded and then unloaded in an ultrahigh vacuum of  $10^{-11}$  torr ( $1.33 \times 10^{-9}$  N/m<sup>2</sup>). Data were obtained under two conditions, very low environmental vibration or deliberate vibration during the loading cycle. These data showed that adhesion occurred in both cases (coefficients of adhesion, 0.11 and 0.19, respectively), in spite of the fact that the specimens were not rigorously cleaned. True stress-strain curves were constructed from data for the contact resistance against the decreasing load for each condition. The general shape of each of the true stress-strain curves was compared with the true stress-strain curve characteristic of the specimen material, and both curves were similar. This similarity suggested that the cold-welded junctions established between the two specimens were formed from the specimen material (copper). Therefore, the observed adhesion was primarily metallic and not a result of adhesion between surface films. The true stress-strain curves showed that specimen vibration reduced the ductility of the junctions, presumably because of extreme work hardening caused by the impulsive forces.

The true stress-strain curves also showed that elastic behavior of the cold-welded junctions occurred as the load was reduced from its maximum value and that considerable plastic deformation of the junctions had occurred when the load was reduced to zero.

The data on contact resistance against load for the vibrated contact seemed to indicate that impulsive forces (vibrations) could increase the area of contact under fixed load to the point where the contact area might revert to an elastic condition.

## INTRODUCTION

The nature of the interface between two metallic surfaces in physical contact is important in the operation of sliding systems because it will determine the friction and wear characteristics of the system. If the surfaces are prevented from coming into intimate physical contact by the presence of an intervening film (a lubricant or contamination), the friction and wear will be relatively low as long as the film remains in place. In the absence of intervening films, the two surfaces will establish asperity contact and cold welding may occur, which creates metallic junctions between the two bodies in contact. When sliding begins, a frictional force arises because these welded junctions must be sheared before relative motion can occur (ref. 1).

Adhesion experiments have been made (refs. 2 to 7) that showed cold welding at the interface between various materials. In these experiments, the two chosen materials were loaded compressively against each other. After unloading, a force was applied in the opposite direction to break the materials apart. The ratio of the breaking force to the loading force defines a dimensionless coefficient of adhesion that serves to indicate the relative adhesion between the various metallic couples under different experimental conditions.

Most of the adhesion experiments are designed to evaluate the possibility of adhesion between couples of various metals and alloys under relatively heavy loads at different temperatures, in air or vacuum. Some experiments, however, have dealt with the phenomena of adhesion on a smaller scale by using smaller specimens and much lighter loads (ref. 5). While these methods may establish a qualitative measure of the adhesion between various materials, they do not reveal much information about the mechanical properties (e. g., ductility, brittle fracture, and creep) of the junctions formed. Furthermore, these experiments reveal little about the behavior at the interface during loading and unloading.

Large-scale tensile-testing procedures cannot be conveniently applied to cold-welded metallic junctions on the asperity level (microjunctions) because of their microscopic nature (extremely small cross-sectional area and length). If these cold-welded junctions could be subjected to tensile testing, judgements on the nature of the junctions formed might be made by comparing junction characteristics (e. g., ductility) to those normally associated with the specimen material. Evidence of marked ductility would also show that metallic cold welding between specimens actually occurs rather than adhesion between surface films.

The objectives of the present experiments is to show that (1) metallic cold-welded junctions are established between two ductile specimens in simple contact, (2) the cold-welded junctions possess the characteristics of the specimen material (e. g., ductility), and (3) the ductility of the junctions is affected by specimen vibration.

These objectives were achieved by (1) measurement of the electrical contact resist-

ance between two oxygen-free high-conductivity (OFHC) copper specimens during loading and unloading in a vacuum of  $10^{-11}$  torr ( $1.33 \times 10^{-9}$  N/m<sup>2</sup>), (2) use of the data obtained during unloading to construct true stress-strain curves, and (3) comparison of the experimental true stress-strain curve to that for the specimen material.

## SYMBOLS

$A_c$	actual contact area between two specimens, mm <sup>2</sup>
$A_r$	reference contact area, mm <sup>2</sup>
$a$	radius of contact area, cm
$b$	pressure coefficient of resistance, cm <sup>2</sup> /kg
$l$	instantaneous length of specimen
$l_0$	initial length of specimen
$\Delta p$	change in pressure, kg/cm <sup>2</sup>
$R_c$	total contact resistance, m $\Omega$
$R_0$	resistance at pressure of 1 atm, m $\Omega$
$R_r$	contact resistance of reference contact area, m $\Omega$
$W$	load, g
$\gamma$	shape factor defined by $\alpha = \gamma a$ and $\beta = a/\gamma$ , where $\alpha$ and $\beta$ are major and minor axis, respectively, of an ellipse
$\epsilon$	true strain, dimensionless
$\rho$	resistivity of specimen material, ohm-cm
$\sigma_T$	true stress, N/m <sup>2</sup>
$\sigma_{TC}$	true stress in contact area, kg/mm <sup>2</sup>

## SPECIMENS

Copper was chosen as the experimental material to fulfill the objectives because it is (1) a very ductile material, (2) easily work hardened, and (3) easily cold welded in a vacuum.

The specimen configuration consisted of a hemispherically tipped rod (9.5-mm diam. by 17.6 mm long) that was loaded against the periphery of a cylinder (50.8-mm diam. by

25.4 mm long). The wall thickness of the cylinder in the contact area was 6.35 millimeters. For these experiments, both specimens were fabricated from commercial OFHC copper and machined to a finish of 8 root mean squares.

## APPARATUS

### Vacuum System

A schematic diagram of the vacuum system used is shown in figure 1. The vacuum chamber is pumped by a 400-liter-per-second ( $0.4\text{-m}^3/\text{sec}$ ) sputter-ion pump and a liquid-nitrogen-cooled titanium sublimation pump. Cryopumping is also available in this chamber and consists of a 20-turn coil of 6.35-millimeter outside diameter stainless-steel tubing through which liquid helium can be circulated. This coil is surrounded by a circular tank that can be filled with liquid nitrogen. The vacuum chamber pressure is measured with a triggered discharge gage.

The vacuum chamber is connected to a rough-pumping manifold by an all-metal, bakable, ultrahigh-vacuum valve. The rough-pumping system consists of a set of three sorption pumps, each connected to the roughing manifold by its own vacuum valve. Roughing pressure is measured by a conventional absolute pressure gage (calibrated in mm Hg) and a thermocouple gage.

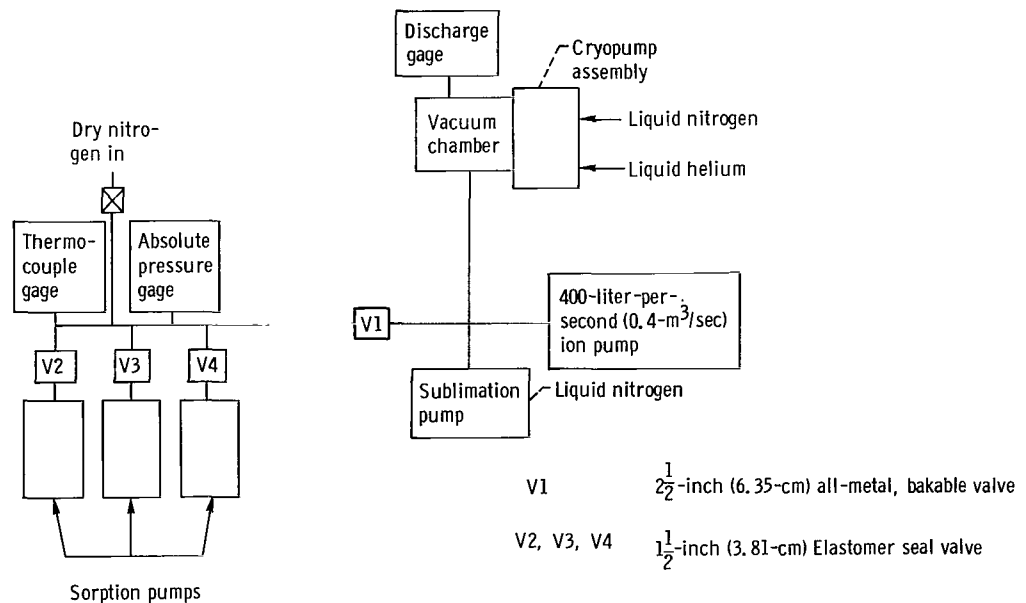


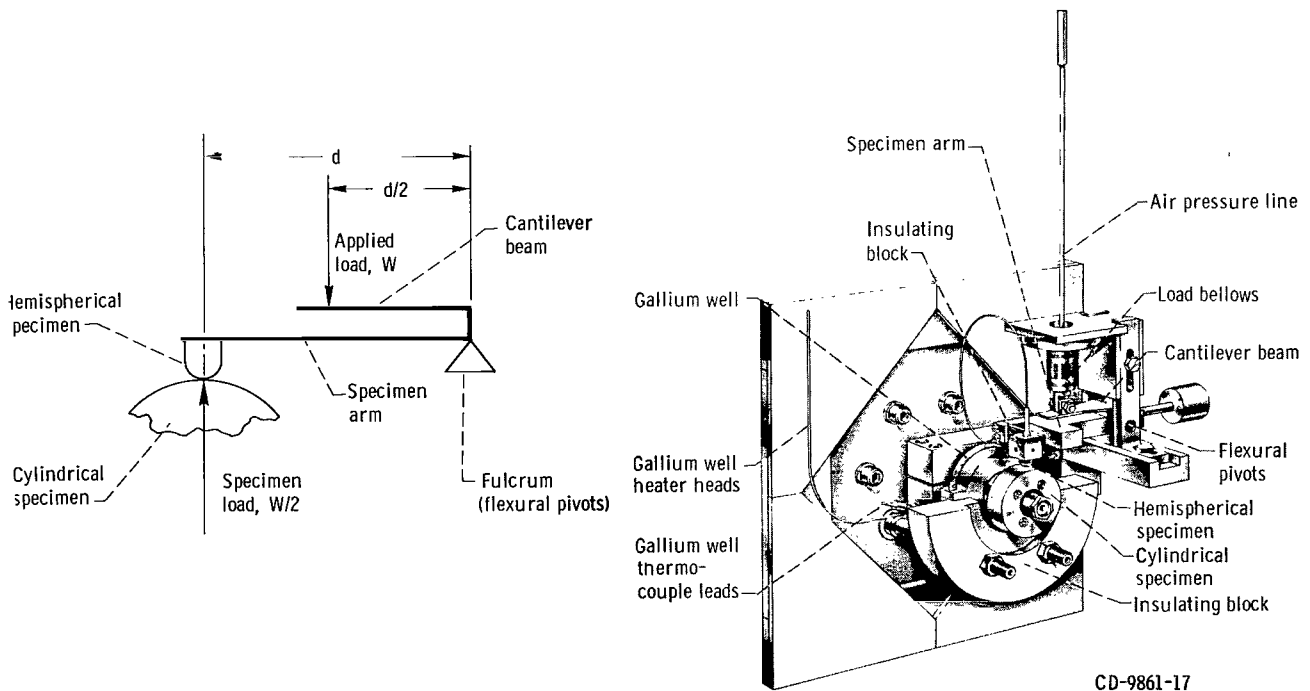
Figure 1. - Block diagram of ultrahigh vacuum system.

Atmospheric pressure is attained by bleeding, into the roughing manifold, nitrogen gas that is first dried by passing through a copper coil immersed in liquid nitrogen.

Bakeout of the vacuum chamber is accomplished by the lowering of an oven enclosure. Bakeout of the 400-liter-per-second ( $0.4\text{-m}^3/\text{sec}$ ) ion pump, the titanium sublimation pump, and associated piping is accomplished by an oven that is permanently installed to enclose these items. Bakeout temperatures are typically 400 K for the vacuum chamber and 400 K for the 400-liter-per-second ( $0.4\text{-m}^3/\text{sec}$ ) ion and sublimation pumps.

## Load System

The specimen loading system is shown schematically in figure 2(a) and photographically in figure 2(b). The specimens are compressively loaded by pressurizing a bellows, located inside the vacuum chamber, with air obtained from a motor-driven air-pressure regulator. The force developed by the pressurized bellows is transmitted through a can-



(a) Schematic diagram of specimen loading system.

(b) Apparatus for measuring static and dynamic contact resistance under various loads.

Figure 2. - Test apparatus for stress-strain behavior experiments.

tiler beam to an arm that holds the stationary specimen in an insulated block. One end of the specimen arm is mounted on two flexural pivots that act as a simple, reliable fulcrum. The form of the loading configuration is a second-class lever with the load applied at the midpoint between the fulcrum and the specimen.

The load-unload cycle, which requires about 20 minutes, is automatically controlled by pressure-sensitive switches. The rate of loading and unloading is approximately 52 grams per minute. Several pounds per square inch are required before the specimens make contact. This arrangement makes available a tensile force (between zero and the pressure required for initial specimen contact) for fracturing the cold-welded junction formed between the specimens. A pressure transducer converts the bellows air pressure to an electrical signal that is used to drive the x-axis of an x, y-recorder.

This loading system allows very smooth compressive loading and unloading of the specimens to permit the interaction of two surfaces to be observed free from the effects of impulsive forces caused by incremental loading.

### Contact-Resistance Measurement

Contact-resistance measurements were made with a commercial four-terminal milliohmmeter. It uses a relatively small alternating test current (40 Hz square wave, 100 mA rms) and a synchronous demodulator, which makes it sensitive only to the test frequency. The instrument is sufficiently sensitive to operate with only 10 microwatts of power applied to the specimens, which reduces the specimen heating. The alternating-current method of resistance measurement also eliminates any errors due to thermal

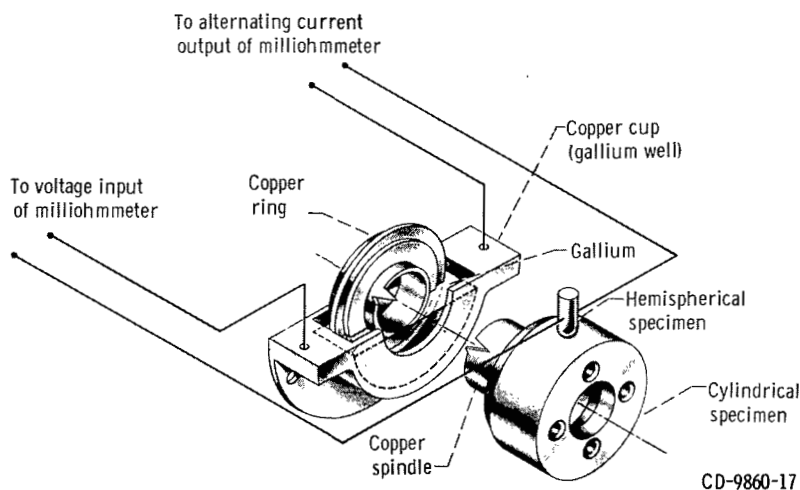


Figure 3. - Schematic diagram of contact-resistance-measuring circuit.

voltages in the measuring circuit. The input and output leads of the milliohmmeter are magnetically shielded to reduce further stray pickup. The direct-current output of the milliohmmeter was connected to the y-axis of the x, y-recorder.

A schematic diagram of the contact-resistance-measuring circuit is shown in figure 3. One current and one voltage lead are secured to the hemispherically tipped specimen by means of a setscrew. The remaining current and voltage leads are connected separately to opposite sides of a copper cup containing gallium. The cylindrical specimen is mounted on one end of an OFHC copper spindle (see fig. 2). A ring machined into the remaining end of the copper spindle and partly immersed in the gallium completes the electrical circuit to the cylindrical specimen.

## Procedure

After the machining, the specimens were washed in a strong detergent solution, rinsed in tap water, briefly dipped into a 20-percent solution of nitric acid ( $\text{HNO}_3$ ), rinsed again in tap water, and submerged in absolute alcohol. The specimens were rinsed several times in acetone prior to insertion into the vacuum chamber. After the test specimens were installed, the vacuum chamber was evacuated and baked out at 400 K for 15 hours. The vacuum system was allowed to cool down to room temperature before the experiments were begun.

The first experiments were conducted under relatively vibration-free conditions. The experiment was initiated by actuation of the loading device, which then increased the air pressure in the bellows to compressively load the specimens against each other. The bellows pressure increased to 15 psi ( $10.4 \times 10^4 \text{ N/m}^2$ ), whereupon the pressure-sensitive switch reversed the pressure-regulator drive. The air pressure in the bellows then decreased to zero where the regulator drive was automatically shutoff. During the loading and unloading cycle, the x, y-recorder produced a plot of contact resistance against load.

In the second type of experiments, external vibrations were deliberately introduced at random during the loading time to determine if vibrations (which could conceivably cause extreme work hardening of the junction) had any effect on the shape of the curve of contact resistance against load during unloading.

New contact areas were used for each experiment.

## THEORETICAL CONSIDERATIONS

### Mechanical Behavior of Contact Area During Loading and Unloading

All machined surfaces are very rough on a microscopic scale. Even the best polishing techniques available today do not produce a smooth surface. The true surface microgeometry is seldom known with any great accuracy, but it generally has a peak and valley appearance (refs. 8 and 9). When two surfaces approach each other, the tips of the highest peaks are the points at which the physical contact between the two surfaces occurs. Since this initial, actual area of contact is very small, the pressure in the contact area is extremely large even under light loads, and the asperities are plastically deformed. The deformation continues until the area of actual contact and the yield strength of the material in the contact spots are sufficient to support the load. The stresses in the asperities are taken up by the bulk of the material supporting them. At some point (under moderate load), the stresses will lie in the elastic range. The end result of these two objects in contact is an actual area of contact consisting of plastically deformed material that is supported by a much greater area consisting of elastically deformed material. Since elastic deformations are completely reversible, those parts of the specimen that were deformed elastically only will regain their original configuration when the load is removed if there is no adhesion (cold welding) between the specimens.

### Elastic Recovery of Specimens with Adhesion

The process of elastic recovery can be restrained by the establishment of metallic junctions (adhesion) between the two specimens (cold welding)(ref. 4). The attempt of the specimens to recover elastically stresses the cold-welded metallic junctions between the two specimens as the applied load is reduced. As the load is reduced gradually, the cold-welded junctions are subjected to a gradually increasing tensile stress. If the total work stored in the elastic deformation of the specimens is not sufficient to fracture all the cold-welded metallic junctions, the specimens will remain adhered to each other. A negative load (tension) can then be gradually applied to the specimens to further stress the cold-welded metallic junctions until they fracture. This entire procedure has all the characteristics of a tensile test of the cold-welded metallic junctions. The problem of developing a true stress-strain curve for these junctions is now resolved to one of measuring the area of contact between the two specimens as the load is increased and then reduced. Once the contact area is known, true stress and strain values at any load can be calculated relative to a reference point.

## Contact-Resistance Measurements and Their Relation to Stress and Strain

Experimental determinations of the actual area of contact between two metallic surfaces under load have utilized several methods, one of which is the measurement of interfacial contact resistance (refs. 1, 6, and 10). Contact-resistance measurements have been used in the past for the study of the phenomenon of adhesion between two lightly loaded specimens (refs. 5 and 11). However, these experiments do not reveal much information about the type or nature of the junctions formed.

The relation between the contact resistance and the radius of the contact area is defined by (ref. 10)

$$R_c = \frac{\rho}{2a} \quad (1)$$

The accuracy of contact-radius calculations derived from contact-resistance measurements is dependent on several conditions: (1) the contact area must be essentially metallic (Ohm's law must be obeyed), (2) the contact area must be at only one point, and (3) the contact area must be essentially circular. The first condition can be satisfied by using clean surfaces and the second and third conditions can be approached by choosing a suitable contact configuration. The magnitude of the errors generated by deviating from these ideal conditions is treated in reference 10.

If the contact resistance and resistivity of the material are known, the radius of a single contact area can be calculated. This basic formula can also be used for an elliptical contact area provided that a shape factor  $\gamma$  is introduced into the calculations (ref. 10). This shape factor relates the constriction resistance of a circular contact area to the constriction resistance of an elliptical contact area. The total contact resistance is then defined by

$$R_c = \frac{\rho}{2a} f(\gamma) \quad (2)$$

The value of  $f(\gamma)$  for various ellipses can be found in reference 10. If the shape factor is near 1, assuming a circular contact area will introduce no great error. This assumption, which is made in this report, greatly simplifies the calculations.

A circular contact area is related to the contact resistance by

$$A_c = \pi \left( \frac{\rho}{2R_c} \right) \quad (3)$$

If the contact resistance at a particular load is measured, true stress in the contact area may be calculated by

$$\sigma_{TC} = \frac{W}{A_c} \quad (4)$$

The true stress in the contact area can be related to the contact resistance when equations (3) and (4) are combined

$$\sigma_{TC} = \frac{4W}{\pi} \left( \frac{R_c}{\rho} \right)^2 \quad (5)$$

True strain can be related to area if the constancy of volume relation (ref. 12) is assumed to give

$$\epsilon = \ln \frac{A_r}{A} \quad (6)$$

A particular point  $A_r$  (the reference area) is chosen so that the strain at any point can be calculated relative to the reference point. The true strain can be related to contact resistance by combining equations (6) and (3)

$$\epsilon = 2 \ln \frac{R_c}{R_r} \quad (7)$$

Thus, equations (5) and (7) can be used to develop a true stress-strain curve for the cold-welded junctions between two specimens from a series of measurements of contact resistance against load during unloading. The developed true stress-strain curve will show whether or not actual metallic junctions are formed. If the true stress-strain curve displays the characteristics of true stress-strain curves obtained from large-scale tensile testing of the specimen materials, metallic junctions have been established.

The values of true stress, true strain, and contact areas calculated from contact-resistance measurements are somewhat uncertain because of the practical difficulties encountered in defining the area of actual contact. All calculations referred to in the discussion are made with the assumption that the conditions under which equation (1) is valid have been satisfied. The values obtained from the calculations cannot be considered absolute. However, they are useful as a means for comparing the data between the two types of experiments. Judgments on the type and nature of the adhesion between the two specimens does not require absolute values and can be made on the basis of the shape of the flow curve alone. Cold-welded metallic junctions should display the characteristics of the specimen materials (e. g. , ductility), whereas adhesion between surface films or metallic junctions containing large amounts of impurities should display characteristics different from those of the specimen materials.

# RESULTS AND DISCUSSION

## Behavior of Vibration-Free Contact Pair

The actual x, y-recorder graphs obtained from the experiments are shown as figures 4 and 5. No discrete points are in these data because the dependent and independent variables are plotted continuously on an x, y-recorder. Arrows were placed on the tracings to show the direction of the trace during the loading and unloading of the specimens.

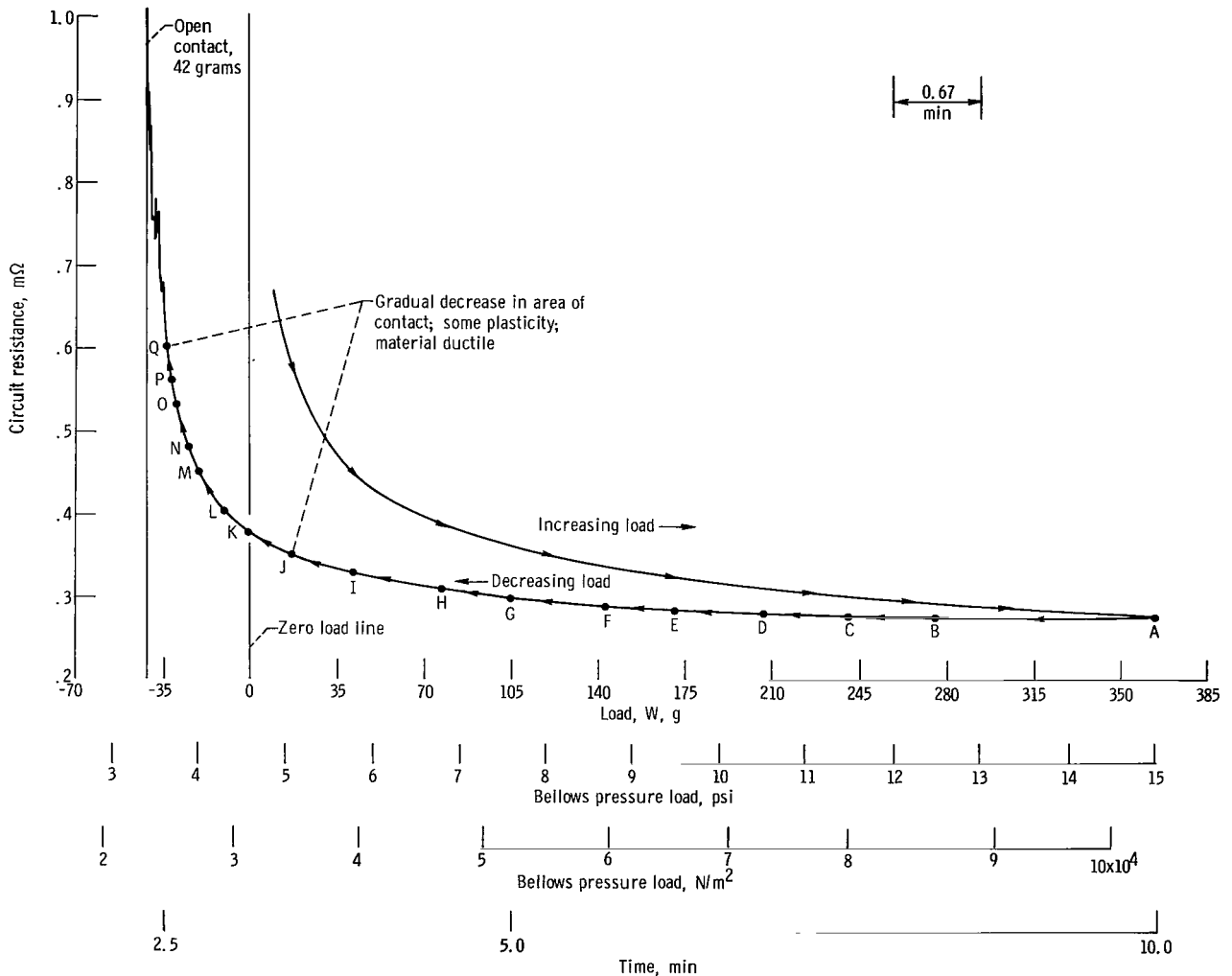


Figure 4. - Actual tracing of contact resistance against load characteristics for oxygen-free high-conductivity copper-copper contact in vacuum in low-vibration environment. Resistance measured with ac milliohm meter; full-scale contact voltage drop, 100 microvolts; full-scale contact power dissipation, 10 microwatts; hemispherical specimen radius, 0.187 inch (4.75 mm); cylindrical specimen diameter, 2 inches (50.8 mm); vacuum,  $10^{-11}$  torr ( $1.33 \times 10^{-9}$  N/m<sup>2</sup>); rate of loading and unloading, 52 grams per minute; peripheral contact.

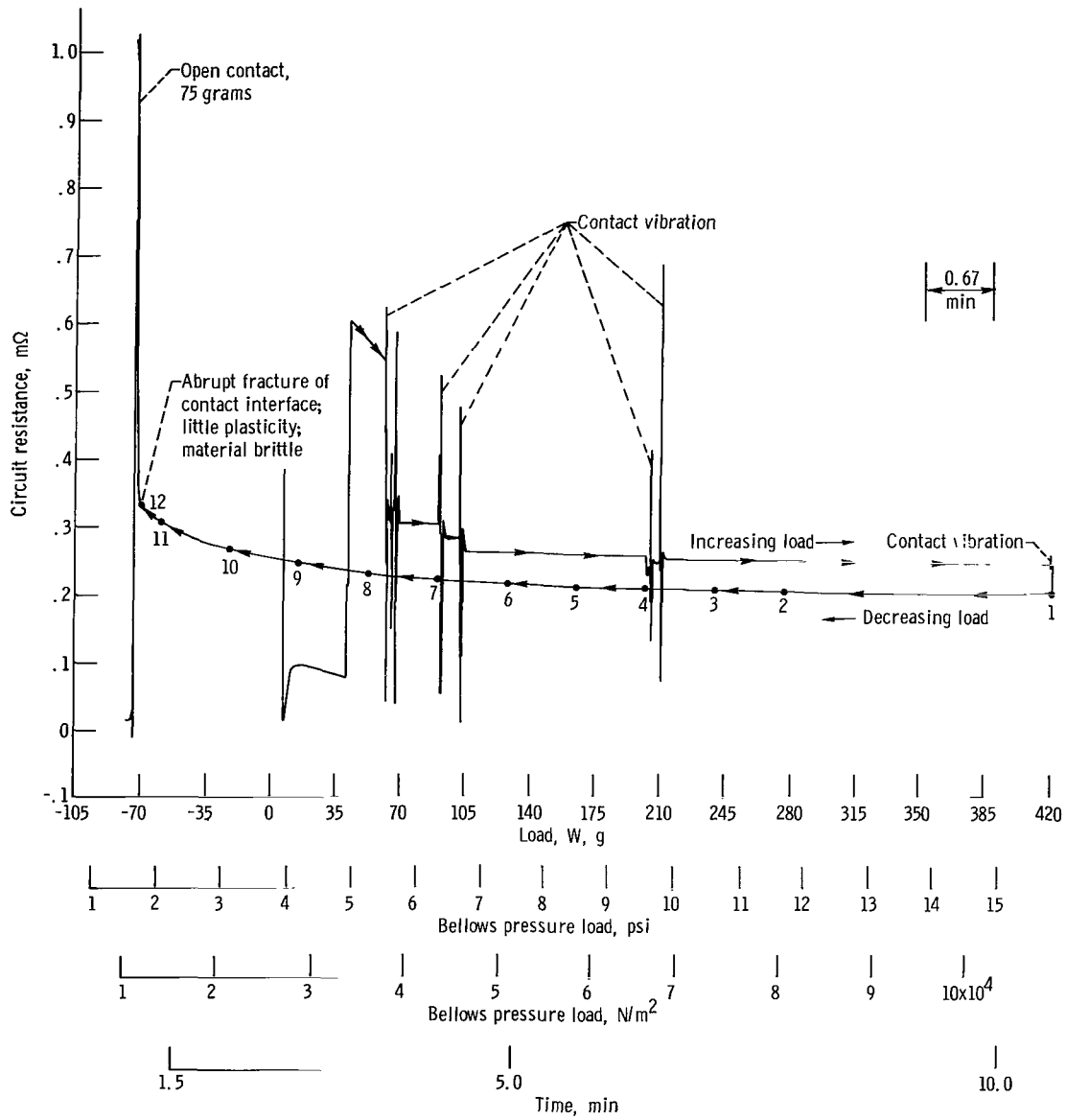


Figure 5. - Actual tracing of contact resistance against load characteristics for oxygen-free high-conductivity copper-copper in vacuum under conditions of contact vibration. Full-scale contact voltage drop, 100 microvolts; full-scale contact power dissipation, 10 microwatts; hemispherical specimen radius, 0.187 inch (4.75 mm); cylindrical specimen diameter, 2 inches (50.8 mm); vacuum,  $10^{-11}$  torr ( $1.33 \times 10^{-9}$  N/m<sup>2</sup>); rate of loading and unloading, 52 grams per minute; peripheral contact.

Figure 4 shows the actual plot of contact resistance (y-axis) against load (x-axis) for an OFHC copper-OFHC copper contact pair in a vacuum of  $10^{-11}$  torr ( $1.33 \times 10^{-9}$  N/m<sup>2</sup>) in a relatively low-vibration environment. As the load was increased, the contact resistance decreased smoothly to a value of 0.278 milliohms at the maximum load of 364 grams. The smoothness of the trace testifies to the success of the vibration reduction efforts. The contact area at this point, calculated by use of equation (1) and a value of  $1.71 \times 10^{-6}$  ohm-centimeter (ref. 13) for the resistivity of copper, is roughly  $3 \times 10^{-3}$  square millimeter. The compressive stress in the calculated contact area at this point is about 120 kilograms per square millimeter. This value is quite high in comparison with the usual values of yield stresses generally given for highly work-hardened copper ( $30 \text{ kg/mm}^2$ , ref. 1). However, asperities are thought to be able to withstand local stresses up to 10 times their normal yield stress (ref. 8), so this value of stress in the contact area would not be unusual.

A value of contact resistance is still shown as the load passes through the zero load point in figure 4. The contact resistance goes to infinity (open contact) only after the application of a tensile force of 42 grams. This result shows that adhesion has occurred between the two OFHC copper specimens in simple contact, in spite of the fact that no effort was expended to secure uncontaminated surfaces. This occurrence is not unusual because adhesion between two copper specimens has also been observed by the author of reference 3 under similar conditions.

The graph of figure 4 also shows that, as the specimens are unloaded, the contact resistance changes smoothly and does not show any abrupt incremental changes until just prior to fracture. This observation suggests that the cold-welded junctions between the specimens are not ruptured immediately by the release of the elastic stresses in the specimens, because the rupture of a junction would cause sharp discontinuities in the trace as a result of incremental increases in contact resistance. However, the extremely small resistance changes due to the rupturing of minute junctions might be beyond the sensitivity of the milliohmmeter.

A true stress-strain curve was developed from the unloading data of figure 4. The points at which the calculations were made are noted by the letters A to Q in figure 4. The values of stress and strain of these points were calculated by use of equations (5) and (7) and point A as a reference. The calculated values were plotted, and the resulting curve is shown in figure 6. Point A was chosen as the zero reference point in figure 6 because the elastic recovery forces of the specimen material were assumed to begin to stress the cold-welded junctions in tension as soon as the external load was reduced. If this assumption is correct, the curve of figure 6 should be similar in appearance to the curve of figure 7.

A comparison of figure 6 (the true stress-strain curve for the cold-welded junctions) and figure 7 (a typical true stress-strain curve for polycrystalline copper obtained by

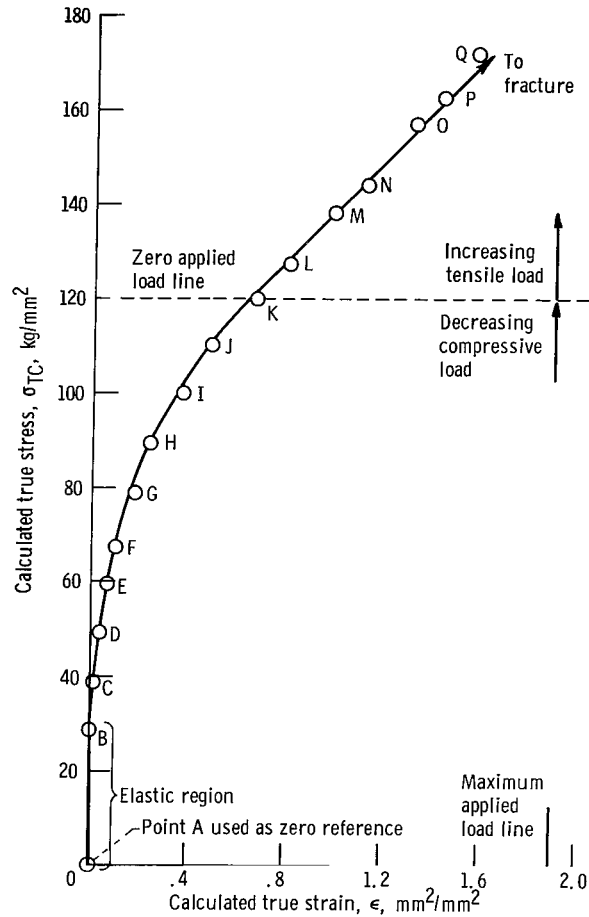


Figure 6. - True stress-strain curve developed from load-resistance measurements displayed in figure 4. Material, oxygen-free high-conductivity copper against itself; vibration-free conditions; rate of unloading, 52 grams per minute.

tensile testing) reveals that the general shapes of the curves are similar, which validates the use of point A as a zero reference point. Both curves show corresponding regions of elasticity (nearly coincidental with the ordinate) and extended plasticity. This similarity suggests that the junctions are formed from the parent material and are not a product of surface contaminants, which leads to the conclusion that truly metallic junctions have been established by adhesion between the specimens (cold-welding) - surface contamination notwithstanding.

Note that the portion of the true stress-strain curve for the cold-welded junctions, which apparently represents elastic behavior (point A to point B in fig. 6), is generated as soon as the load is reduced from its maximum value and not around the zero external load point. At the zero external load point, the curve of figure 6 shows that considerable plastic deformation of the cold-welded junctions has occurred.

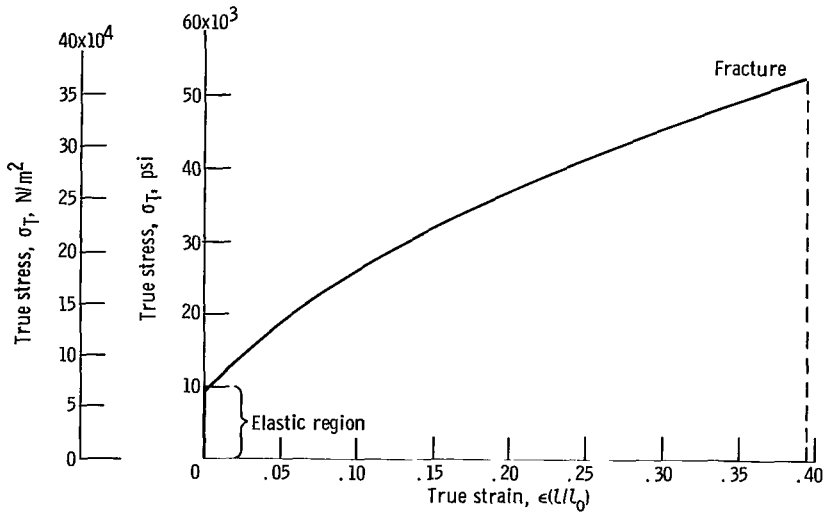


Figure 7. - True stress-strain curve for polycrystalline copper (ref. 14).

## Behavior of Contact Pair with Vibration

Figure 5 shows the contact-resistance-against-load data for OFHC copper specimens that were deliberately subjected to vibration at random times during the compressive loading cycle only. The effect of the vibrations can be seen on the graph as sharp fluctuations in contact resistance succeeded by an instantaneous decrease in contact resistance. The lower value of contact resistance indicates an increase in the actual area of contact. This increase is not the result of a change in the resistivity of the material by work hardening because work hardening causes an increase in resistivity (ref. 13), which is in direct opposition to the observed data. The additional area of actual contact caused by the vibrations is obviously in excess of that required to support the static load. The static load has remained essentially constant during the period of vibration, so the result of the increased area of contact is a decrease of stress in the contact area. The lowered stresses will be below the value required for continued plastic deformation. In fact, a greater stress will now be required for plastic deformation because of work hardening, so it is conceivable that the lowered stress might be in the elastic range of the material immediately after the vibration has increased the area of contact.

The slope of the trace in figure 5 succeeding the fluctuations caused by the vibrations seem to point to elastic behavior. The slope of the trace is near zero (nearly constant contact resistance), which means that the change in the contact area is very small (for a given increment of load). The resulting strain must also be very small because strain is related to changes in area by equation (6). Since small strains are a characteristic of elastic behavior for metals, those portions of the trace having nearly zero slope

might represent elastic behavior of the material.

The experiment represented by figure 5 was loaded to a maximum load of 390 grams. The contact resistance at maximum load prior to specimen vibration was 0.241 milliohms, which corresponded to a calculated actual contact area of about  $4 \times 10^{-3}$  square millimeter. The stress in this area at maximum load was about 98 kilograms per square millimeter. The specimens were also vibrated at maximum load, whereupon the contact resistance decreased to 0.2 milliohm, which corresponded to a calculated actual contact area of  $5.75 \times 10^{-3}$  square millimeter. Since the load remained the same, the stress in the contact area decreased to 67.7 kilograms per square millimeter because of the increased contact area.

The decreasing load portion of the trace in figure 5 has two outstanding dissimilarities to that in figure 4: (1) the slope of the trace in figure 5 increases more slowly as the cold-welded junctions approach the point of fracture, and (2) the contact resistance increases abruptly (fracture point) after having changed little from its value at maximum load. This behavior is unlike that displayed in figure 4, which shows relatively large changes in slope and contact resistance between maximum load and the fracture point.

A tensile force of about 75 grams was required to separate the specimens subjected to vibration during loading. The coefficient of adhesion for these specimens is 0.19,

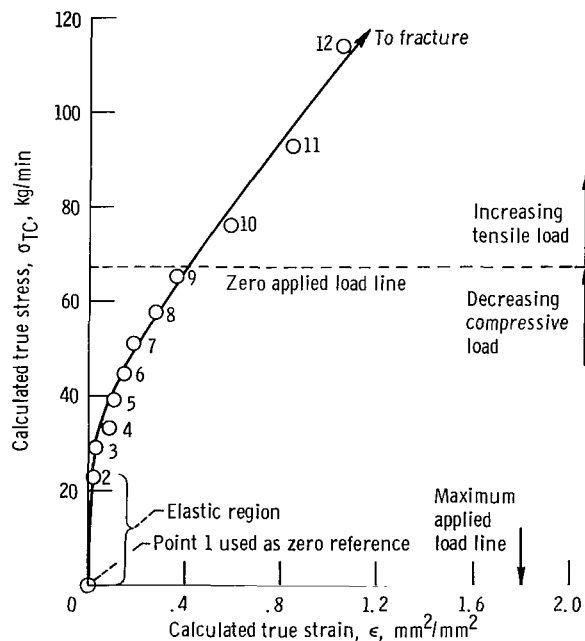


Figure 8. - True stress-strain curve developed from load-resistance measurements displayed in figure 5. Material, oxygen-free high-conductivity copper against itself; contact-vibration conditions; rate of unloading, 52 grams per minute.

TABLE I. - EXPERIMENTAL AND CALCULATED VALUES OBTAINED FROM VIBRATION-FREE AND VIBRATED STATIONARY OXYGEN-FREE HIGH-CONDUCTIVITY COPPER CONTACT PAIRS IN VACUUM OF  $10^{-11}$  TORR ( $1.33 \times 10^{-9}$  N/m<sup>2</sup>)

Specimen condition during test	Maximum load, W, g	Calculated strain prior to fracture, $\epsilon$ , mm <sup>2</sup> /mm <sup>2</sup>	Coefficient of adhesion	Contact resistance at maximum load, m $\Omega$	Calculated actual area of contact, A <sub>c</sub> , mm <sup>2</sup>	Calculated stress at maximum load, $\sigma_T$ , kg/mm <sup>2</sup>
Vibration-free	360	1.56	0.11	0.275	0.00300	120
Vibration during loading cycle	389	1.05	0.19	<sup>a, b</sup> 0.241	<sup>b</sup> 0.00396	<sup>b</sup> 98.2
				<sup>a, c</sup> 0.200	<sup>c</sup> 0.00575	<sup>c</sup> 67.7

<sup>a</sup>Specimens vibrated at maximum load.

<sup>b</sup>Value prior to vibration.

<sup>c</sup>Value after vibration.

which is about twice that of the specimens maintained in a vibration-free environment. The appearance of the trace in figure 5 is suggestive of a rather brittle material (little contact-resistance change, abrupt fracture) in contrast to the trace of figure 4, which is suggestive of a ductile material (large contact-resistance change, deliberate fracture). The brittle behavior of the junctions is thought to result from the extreme work hardening of the junctions by the vibration forces.

Stress and strain calculations at the points indicated (1 to 12) in figure 5 were made relative to point 1 (for the same reason discussed in the section Behavior of Vibration-Free Contact Pair), and the results are plotted in figure 8. This curve is similar to that of figure 6, and the same conclusions apply. However, the calculated strain just prior to fracture is significantly less, which shows that the junctions do not have the amount of ductility that the undisturbed junctions had.

A summary of the important experimental and calculated values for the two experimental conditions is given in table I.

## CONCLUDING REMARKS

Electrical contact-resistance measurements can be employed to show the mechanical behavior of the contact region between two metallic specimens in physical contact during loading and unloading. Although the basic data itself exposes the mechanical behavior of

the contact area, it is better displayed by means of true stress-strain curves that can be constructed from the data for contact resistance against load. The calculated values used to construct the true stress-strain curves cannot be considered absolute because of the practical difficulties encountered in defining the geometry of the actual contact area. However, the general shape of these curves developed from the basic data is quite useful.

A similarity exists between each constructed true stress-strain curve and the characteristic true stress-strain curve for the specimen material (polycrystalline copper). This similarity shows that the cold-welded junctions formed between the two specimens under both vibration-free and vibrated conditions are formed from the specimen material. It can be concluded that actual metallic adhesion between the oxygen-free high-conductivity (OFHC) copper specimens in simple contact occurs in spite of relatively unclean surfaces, but the coefficient of adhesion is relatively low (vibration-free contact, 0.11; vibrated contact, 0.19).

A comparison of the true stress-strain curves for the vibration-free and vibrated conditions showed that the cold-welded junctions formed by the vibration-free contact pair had more ductility (larger strain before fracture) than those formed by the vibrated contact pair (smaller strain before fracture). This decreased ductility is thought to be caused by the extreme work hardening of the junction by the vibrational forces.

Both true stress-strain curves also show that elastic deformation of the junctions occurs immediately on reduction of the load from its maximum value. When the load is reduced to zero, both true stress-strain curves show that considerable plastic deformation of the cold-welded junctions has occurred.

When the specimens were vibrated during the loading cycle, an instantaneous increase in contact area occurred. The flat slope of the curve of contact resistance against load immediately following the vibration suggests that the contact area has increased to a value where the stresses in the contact region might now be below the yield stress of the material. Contact area deformation might now be elastic again for a time succeeding the vibration, rather than continued plastic. The reason for this behavior is that the contact area has become through vibration more than that required to support the static load.

When this information is applied to static electrical contacts (e. g., relays), it suggests that the contacts, which close with some impact and vibration, probably deform only elastically after a few closures; the impact and vibration will have enlarged the contact area to more than that required to support the load.

Lewis Research Center,  
National Aeronautics and Space Administration,  
Cleveland, Ohio, May 24, 1968,  
129-03-13-02-22.

## REFERENCES

1. Bowden, F. P.; and Tabor, D.: The Friction and Lubrication of Solids. Vol. I. Clarendon Press, Oxford, 1958.
2. Sikorski, M. E.: Correlation of the Coefficient of Adhesion with Various Physical and Mechanical Properties of Metals. *J. Basic Eng.*, vol. 85, no. 2, June 1963, pp. 279-285.
3. Buckley, Donald H.; and Johnson, Robert L.: Friction, Wear, and Adhesion Characteristics of Titanium-Aluminum Alloys in Vacuum. NASA TN D-3235, 1966.
4. Bowden, F. P.; and Rowe, G. W.: The Adhesion of Clean Metals. *Proc. Roy. Soc.*, ser. A, vol. 233, no. 1195, Jan 10, 1956, pp. 429-442.
5. Johnson, K. I.; and Keller, D. V., Jr.: Effect of Contamination on the Adhesion of Metallic Couples in Ultra-High Vacuum. *J. Appl. Phys.*, vol. 38, no. 4, Mar. 15, 1967, pp. 1896-1904.
6. Hordon, M. J.: A Study of the Adhesion and Cohesion of Metals. National Research Corp. (NASA CR-85864), Mar. 9, 1967.
7. Winslow, P. M.; and McIntyre, D. V.: Adhesion of Metals in the Space Environment. *J. Vac. Sci. Tech.*, vol. 3, no. 2, Mar.-Apr. 1966, pp. 54-61.
8. Williamson, J. P. B.: Topography of Solid Surfaces. Paper presented at the NASA Symposium on the Interdisciplinary Approach to Friction and Wear, San Antonio, Texas, Nov. 1967.
9. Greenwood, J. A.; and Williamson, J. P. B.: Contact of Nominally Flat Surfaces. *Proc. Roy. Soc.*, ser. A, vol. 295, no. 1442, Dec. 6, 1966, pp. 300-319.
10. Holm, Ragnar: Electric Contacts Handbook. Third ed., Springer-Verlag, Berlin, 1958.
11. Keller, D. V., Jr.; and McNicholas, T.: Adhesion Between Atomically Pure Metallic Surfaces, Part IV. Rep. MET-1100-6801-SA, Syracuse Univ. Res. Inst., Dept. Chem. Eng. and Metallurgy, Jan. 1968.
12. Dieter, George E., Jr.: Mechanical Metallurgy. McGraw-Hill Book Co., Inc., 1961.
13. Lyman, Taylor, ed.: Properties and Selection of Metals. Vol. 1 of Metals Handbook. Eighth ed., ASM, 1961.

14. Hayden, W.; Moffatt, William G.; and Wulff, John: Vol. 3 of Structure and Properties of Materials. Mechanical Behavior. John Wiley & Sons, Inc., 1965, p. 8.

FIRST CLASS MAIL

ILL 001 42 51 3DS 68216 00903  
AIR FORCE WEAPONS LABORATORY/AWL/7  
KIRTLAND AIR FORCE BASE, NEW MEXICO 87117

SEE LIST OF PUBLICATIONS ACTIVITY FOR THE YEAR 1978

POSTMASTER: If Undeliverable (Section 158  
Postal Manual) Do Not Return

*"The aeronautical and space activities of the United States shall be conducted so as to contribute . . . to the expansion of human knowledge of phenomena in the atmosphere and space. The Administration shall provide for the widest practicable and appropriate dissemination of information concerning its activities and the results thereof."*

— NATIONAL AERONAUTICS AND SPACE ACT OF 1958

## NASA SCIENTIFIC AND TECHNICAL PUBLICATIONS

**TECHNICAL REPORTS:** Scientific and technical information considered important, complete, and a lasting contribution to existing knowledge.

**TECHNICAL NOTES:** Information less broad in scope but nevertheless of importance as a contribution to existing knowledge.

**TECHNICAL MEMORANDUMS:** Information receiving limited distribution because of preliminary data, security classification, or other reasons.

**CONTRACTOR REPORTS:** Scientific and technical information generated under a NASA contract or grant and considered an important contribution to existing knowledge.

**TECHNICAL TRANSLATIONS:** Information published in a foreign language considered to merit NASA distribution in English.

**SPECIAL PUBLICATIONS:** Information derived from or of value to NASA activities. Publications include conference proceedings, monographs, data compilations, handbooks, sourcebooks, and special bibliographies.

**TECHNOLOGY UTILIZATION PUBLICATIONS:** Information on technology used by NASA that may be of particular interest in commercial and other non-aerospace applications. Publications include Tech Briefs, Technology Utilization Reports and Notes, and Technology Surveys.

*Details on the availability of these publications may be obtained from:*

**SCIENTIFIC AND TECHNICAL INFORMATION DIVISION  
NATIONAL AERONAUTICS AND SPACE ADMINISTRATION  
Washington, D.C. 20546**